



# Parametric study of a concentric coaxial glass tube solar air collector: a theoretical approach

Vishal Dabra<sup>1</sup> · Avadhesh Yadav<sup>1</sup>

Received: 4 May 2017 / Accepted: 29 November 2017 / Published online: 17 December 2017  
© Springer-Verlag GmbH Germany, part of Springer Nature 2017

## Abstract

Concentric coaxial glass tube solar air collector (CCGTSAC) is a quite innovative development in the field of solar collectors. This type of collector is specially designed to produce hot air. A mathematical model based on the energy conservation equations for small control volumes along the axial direction of concentric coaxial glass tube (CCGT) is developed in this paper. It is applied to predict the effect of thirteen different parameters on the exit air temperature rise and appeared that absorber tube size, length of CCGT, absorptivity of transparent glazing, transmissivity of transparent glazing, absorptivity of absorber coating, inlet or ambient air temperature, mass flow rate, variation of thermo-physical properties of air, wind speed, solar intensity and vacuum present between transparent glazing and absorber tube are significant parameters. Results of the model were analysed to predict the effect of key parameters on the thermal performance of a CCGTSAC for exit air temperature rise about 43.9–58.4 °C.

## Nomenclature

$C_p$	Specific heat of air (J/kgK)
$D_1$	Transparent glazing radius (m)
$D_2$	Absorber tube radius (m)
$G$	Solar intensity ( $W/m^2$ )
$h_1$	Heat transfer coefficient from absorber coating to transparent glazing ( $W/m^2K$ )
$h_2$	Heat transfer coefficient from absorber glass tube to exit air ( $W/m^2K$ )
$h_a$	Heat transfer coefficient from transparent glazing to ambient air ( $W/m^2K$ )
$j$	Element along the tube axis(–)
$K_g$	Thermal conductivity of glass ( $W/mK$ )
$L$	Length of CCGT (m)
$\dot{m}$	Mass flow rate of air (kg/Sec)
$N$	Total number of elements (–)
$Nu$	Nusselt number(–)
$Pr$	Prandtl number (–)
$Re$	Reynolds number(–)
$r_1$	Transparent glazing radius (m)
$r_2$	Absorber tube radius (m)
$t$	Thickness of absorber tube (m)
$T_a$	Ambient temperature (°C)
$T_{inlet}$	Inlet air temperature (°C)
$T_{outlet}$	Exit air temperature (°C)
$T_{exp}$	Experimentally calculated exit air temperature (°C)
$T_{sim}$	Simulated calculated exit air temperature (°C)
$T_1$	Transparent glazing temperature (°C)

$T_2$	Absorber coating temperature (°C)
$T_3$	Absorber glass tube (°C)
$T_4$	Fluid temperature (°C)
$u_{wind}$	Wind speed (m/Sec)

## Greek symbols

$\alpha_1$	Absorptivity of transparent glazing (–)
$\alpha_2$	Absorptivity of absorber tube (–)
$\rho$	Density of air ( $kg/m^3$ )
$\epsilon_1$	Emissivity of transparent glazing (–)
$\epsilon_2$	Emissivity of absorber coating (–)
$\epsilon_{12}$	Interchange factor (–)
$\mu$	Kinematic viscosity of the air (kg/msec)
$\Delta x$	Length of a slice along the tube axis (m)
$K$	Thermal conductivity of air ( $W/m^2K$ )
$\tau_1$	Transmissivity of transparent glazing (–)
$\sigma$	Stefan's Boltzmann constant( $W/m^2K^4$ )

## Abbreviations

CCGT	Concentric coaxial glass tube
CPC	Compound parabolic concentrator
ETC	Evacuated tube collector
HTF	Heat transfer fluid

## 1 Introduction

Solar air collectors are broadly using solar energy conversion devices employed to deliver hot air at low to moderate temperatures for space heating and drying agricultural products such as fruits, seeds, vegetables etc. [1–3]. There are several types of different solar air collector in the literature. But these collectors seize some limitations in their thermal capacity. Such solar air collector has low thermal efficiency because

✉ Vishal Dabra  
vishaldabra16787@gmail.com

<sup>1</sup> Department of Mechanical Engineering, National Institute of Technology, Kurukshetra 136119, India

of low convective heat transfer coefficient between the absorber surface and air leading to the higher temperature of the absorber surface, which results in higher heat losses to the surroundings. Top losses of the solar air collectors were a function of glazing temperature, emissivity of the glazing, wind speed and ambient temperature [4–6]. Akpınar and Kocıyigit [7] suggested that the thermal performance of the solar air collectors depends significantly on the solar radiation, the contour of the absorber and extension of the air flow line and Sahin [8] suggested that thermal performance of solar air collectors also depends on several parameters such as inlet air temperature, air velocity, collector slope and properties related to collector. Yang et al. [9] suggested methods for improving the thermal performance of solar air collector on the basis of the critical parameter sensitivity analysis. Roughness parameters had a strong influence to increase the heat transfer coefficient between the absorber surface and HTF [10, 11]. Harding and Window [12] investigated the degradation of the thermal performance of evacuated tube solar collector by the presence of low pressure gas in the annular space. El-Nashar [13] investigated the influence of dust deposition on a large field of evacuated tube collectors on the thermal performance of the plant. Tang et al. [14] suggested that climatic conditions had a negligible effect on the diurnal thermal performance of ETC due to less heat loss of the collector to the ambient air. Gao et al. [15] investigated the best possible flow rate of HTF for getting maximum heat gain with different meteorological conditions. Kim and Seo [16] investigated the affected of the shape of the absorber, incidence angle of solar irradiation, and arrangement of collector tubes. Ma et al. [17] evaluated a key parameter of glass evacuated tube solar collector was the surface temperature of the absorbing coating. Fischer et al. [18] developed a model to investigate the thermal performance of solar collector by characterizing the transmission of irradiance through glazing and absorption of irradiance by the absorber. Ares-Muzio et al. [19] designed a solar collector with both end open evacuated tube and studied the absorption characteristics of the collector. Wang et al. [20] enhanced the solar transmittance of glazing tubes of ETC for 0.94 by using a porous SiO<sub>2</sub> antireflection coating. Hall and blower [21] developed a solar collector with a high absorptivity and a low-emissivity. Dabra et al. [22] suggested that thermal performance of the evacuated tube solar air collector improved by using a flat reflector. Garcia-Valladares and Velazquez [23] simulated a single pass solar collector for enhancing the thermal performance and fluid-dynamic behaviour by using CPC. Li and Wang [24] used Water and N<sub>2</sub> as working fluid in an evacuated tube solar collector with CPC. Zhang and Yamaguchi [25] proposed a solar collector using supercritical CO<sub>2</sub> as the working fluid and investigated temperature and flow rate in the collector. Zhao et al. [26] studied the different flow conditions inside the horizontal ETC by

varying the temperature at different inlets of evacuated tube and diameters of the evacuated tube. Shah and Furbo [27] developed a modelled with three different tube lengths varying from 0.59 m to 1.47 m and investigated thermal performance at different mass flow rates varying from 0.05 kg/min to 10 kg/min with a constant inlet temperature of 60 °C. An experimental setup of a solar air collector was developed and suggested that the mass flow rate of the air was directly proportional to collector performance [28, 29]. Naik et al. [30] developed a mathematical model to predict the exit temperature of different working fluids and investigated the effect of different parameters on the thermal performance of the system.

Based on the published works, sufficient literature is available on the parametric behaviour of flat plate and evacuated tube solar air collector. Some parameters are not considered in the literature but have significant effect on the performance of CCGTSAC. Therefore, there is a need for additional studies on the CCGTSAC for enhancing their performance. The purpose of this paper is to study the influence of parameters on the performance of CCGTSAC.

## 2 Mathematical formulation

Before the establishment of mathematical model, the following general assumptions will be made in the process of the energy balance analysis to the heat characteristics and structural features of the CCGT as shown in Fig. 1.

1. CCGT is operating under steady state condition.
2. CCGT is used for flow passage and HTF is assumed to be air.
3. The air flow inside the CCGT has a uniform velocity.
4. There is no leakage of air from the CCGT.
5. The temperature varies only along the airflow direction.
6. The temperature gradient along the radial direction of the CCGT is negligible.
7. Heat transfer coefficients and area distribution are assumed to be uniform and constant.
8. During the test process, the solar radiation falling on the CCGT is assumed to be distributed uniformly.

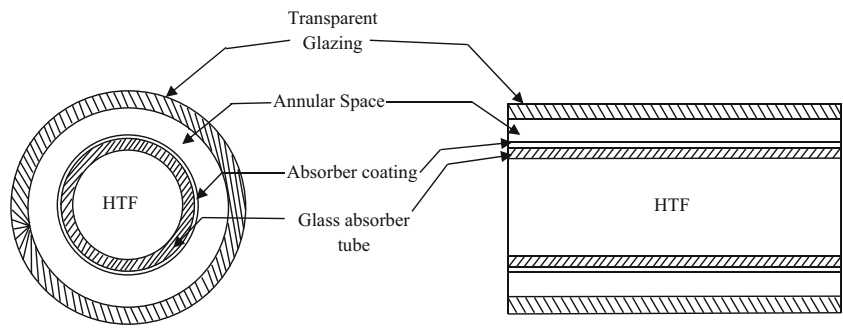
The energy balance equations for each component of CCGTSAC can be written as follows

For transparent glazing

$$a_1 T_1^4 + b_1 T_1 + c_1 T_2^4 + d_1 T_2 + g_1 = 0 \quad (1)$$

For absorber coating

**Fig. 1** Cross-sectional views of concentric coaxial glass tube



$$a_2T_1^4 + b_2T_1 + c_2T_2^4 + d_2T_2 + e_2T_3 + g_2 = 0 \tag{2}$$

For glass absorber tube

$$d_3T_2 + e_3T_3 + f_3T_4 = 0 \tag{3}$$

Heat transfer fluid

$$\frac{dT_4}{dx} = h_4(T_3 - T_4) \tag{4}$$

Where,  $T_1, T_2, T_3$  and  $T_4$  are temperatures of various components as shown in Fig. 2. These are functions of CCGT length and  $a_i, b_i, c_i, d_i, e_i, f_i, g_i$  and  $h_i$  are coefficients with  $i = 1, \dots, 4$ . These coefficients involve the thermo-physical properties of the fluid, geometric properties of the CCGT and climatic conditions. The values of coefficients are expressed in the following expressions.

$$a_1 = \left( \frac{r_2\sigma}{\epsilon_{12}} \right) + r_2\sigma\epsilon_1 \tag{5}$$

$$b_1 = h_1r_2 + h_ar_1 \tag{6}$$

$$c_1 = -\frac{r_2\sigma}{\epsilon_{12}} \tag{7}$$

$$d_1 = h_1r_2 \tag{8}$$

$$g_1 = -(h_ar_1T_a + r_1\sigma\epsilon_1T_a^4 + G\alpha_1r_1) \tag{9}$$

$$a_2 = \frac{r_2\sigma}{\epsilon_{12}} \tag{10}$$

$$b_2 = h_1r_2 \tag{11}$$

$$c_2 = -\frac{r_2\sigma}{\epsilon_{12}} \tag{12}$$

$$d_2 = \frac{K_g}{\ln\left(1 + \frac{t}{r_2}\right)} - h_1r_2 \tag{13}$$

$$e_2 = \frac{K_g}{\ln\left(1 + \frac{t}{r_2}\right)} \tag{14}$$

$$g_2 = G\tau_1\alpha_2r_2 \tag{15}$$

$$d_3 = \frac{K_g}{\ln\left(1 + \frac{t}{r_2}\right)} \tag{16}$$

$$e_3 = \frac{K_g}{\ln\left(1 + \frac{t}{r_2}\right)} - h_2r_2 \tag{17}$$

$$f_3 = h_2r_2 \tag{18}$$

$$h_4 = \frac{2\pi r_2 h_2}{mC_p} \tag{19}$$

The values of different heat transfer coefficients are normally calculated from the following relations [35–].

Heat transfer coefficient from transparent glazing to ambient

$$h_a = \frac{Nu \times K_a}{D_1} \tag{20}$$

$$Nu = C_1 Re^n \tag{21}$$

Where,

$$C_1 = 0.615 \& n = 0.466 \quad 40 < Re < 4000,$$

$$C_1 = 0.174 \& n = 0.618 \quad 4000 < Re < 40000,$$

$$C_1 = 0.0239 \& n = 0.805 \quad 40000 < Re < 400000$$

Heat transfer coefficient from absorber tube to transparent glazing

$$h_1 = 0.026 \text{ W/m}^2\text{K (with vacuum) and } 5 \text{ W/m}^2\text{K (without vacuum)} \tag{22}$$

Heat transfer coefficient from absorber tube to flowing air

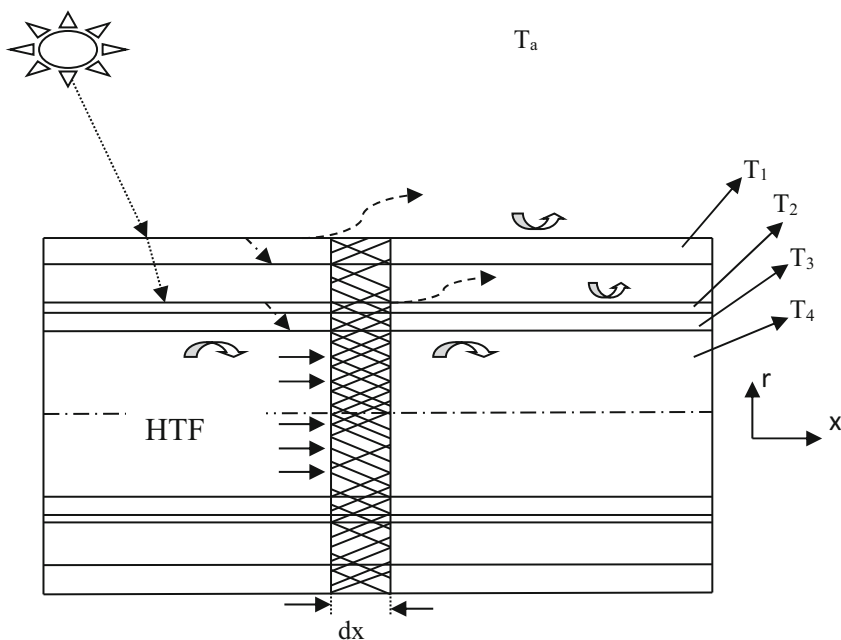
$$h_2 = \frac{Nu \times K_a}{D_2} \tag{23}$$

$$Nu = 0.0214(Re^{0.8} - 100)Pr^{0.4} \tag{24}$$

When  $0.5 < Pr < 1.5$  &  $10^4 < Re < 5 \times 10^6$ .

These four energy balance equations are coupled and solved numerically by using all given relations.

**Fig. 2** Schematic diagram of the concentric coaxial glass tube with heat transfer mechanism



**Mode of heat transfer Symbols used**

**Conduction**



**Convection**



**Radiation**



The physical properties of fluid are assumed to vary linearly with temperature within the range encountered in solar air heaters. Therefore, typical linear equations for the viscosity, density, thermal conductivity and specific heat of air are implemented in the theoretical procedure. The following are assumed for [4, 35, 36].

$$\mu = [1.983 + 0.00184(T_{in}-27)] \times 10^{-5} \tag{25}$$

$$\rho = 1.1774 - 0.00359(T_{in}-27) \tag{26}$$

$$k = 0.02624 + 0.0000758(T_{in}-27) \tag{27}$$

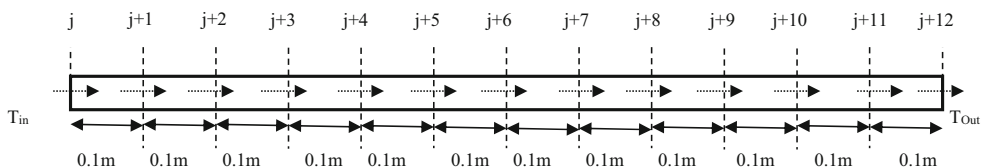
$$C_p = 1.0057 + 0.000066(T_{in}-27) \tag{28}$$

**3 Method of solution**

For obtaining precise results, the collector is divided into *N* fine horizontal elements in order to solve the system on every element while considering that the exit of the *j*th element is the entrance for the following element as shown in Fig. 3. The energy conservation equations are solved by using the iterative numerical method. The axial coordinate is approximated as  $x = j\Delta x$ ,  $j = 0, 1, 2, 3, \dots, N$ . Then  $T_1(x) = T_1(j\Delta x) = T_{1,j}$ . Similarly for  $T_{2,j}$ ,  $T_{3,j}$ , and  $T_{4,j}$ . For the initial boundary condition  $j = 0$  at  $x = 0$ ,  $T_4(0) = T_{4,0}$ . With this value, and using the iterative numerical method to solve the set of equations, the values of  $T_{3,0}$ ,  $T_{2,0}$  and  $T_{1,0}$  are found. Now, by applying the Euler method to Eq. 4,  $T_{4,j+1}$  is obtained as

$$T_{4,j+1} = T_{4,j} - H_4(T_{3,j} - T_{4,j}) \tag{29}$$

**Fig. 3** Schematic diagram of collector element



Where  $H_4 = (\Delta x) \times (h_4)$  (30)

Substituting the values of  $T_{3,0}$  and  $T_{4,0}$  in Eq. 29,  $T_{4,1}$  is obtained. Similarly, the values of  $T_{4,2}$ ,  $T_{4,3}$ ,..... $T_{4,13}$  can be obtained.

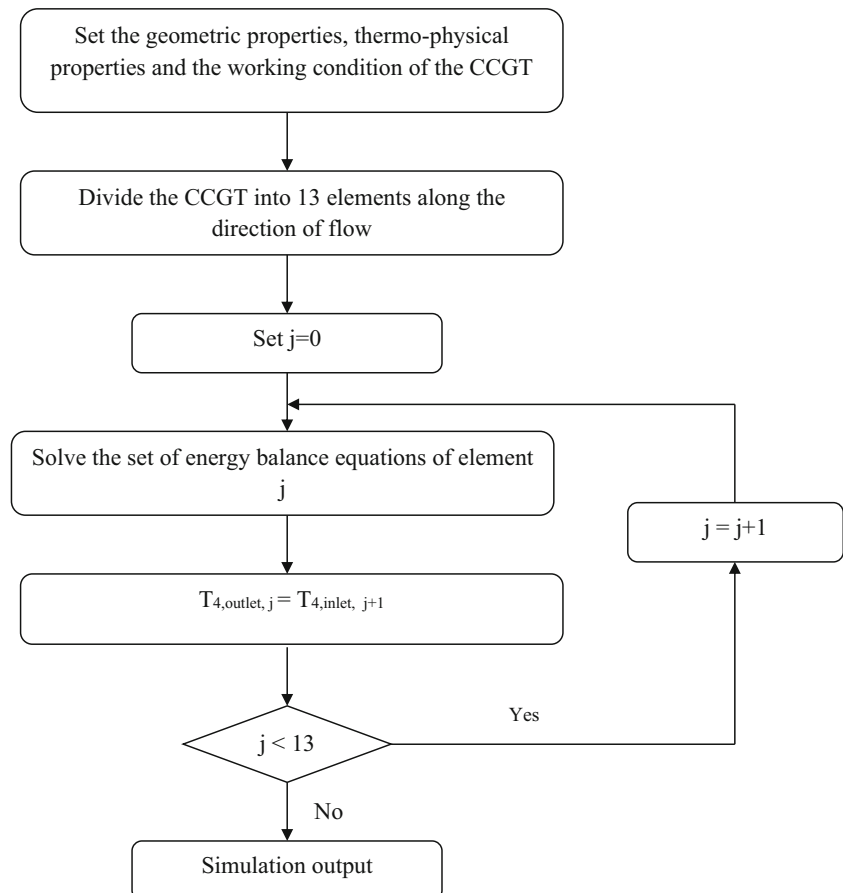
A program of resolution on JAVA language has been developed for this problem and procedure is employed to solve the energy balance equations at different elements along the length of CCGT as shown in Fig. 4.

## 4 Experimental setup and test

To validate the above JAVA simulation program an experimental setup of a CCGT is mounted at NIT Kurukshetra, India [29°58' (latitude) north and 76°53' (longitude) east].

A CCGT was installed on a rigid iron frame and tilted at 30° relative to horizontal surface with south facing shown in Fig. 5 and material used in fabrication of CCGT is listed in Table 1. The air flow measurement is taken with anemometer of model AM-4208 with an accuracy of  $\pm 2\%$  and resolution of 0.1 m/Sec. The incident solar radiation is measured by a pyranometer of model CM 11, Kipp and Zonen, Holland with an accuracy of  $\pm 2 \text{ W/m}^2$  and resolution of  $1 \text{ W/m}^2$ . Finally,

**Fig. 4** Flow diagram for JAVA code



RTD PT 100 temperature sensors are used to measure temperature of air at different points. The temperature sensors are connected to a digital temperature indicator that gives the temperature with a resolution of  $0.1 \text{ }^\circ\text{C}$ .

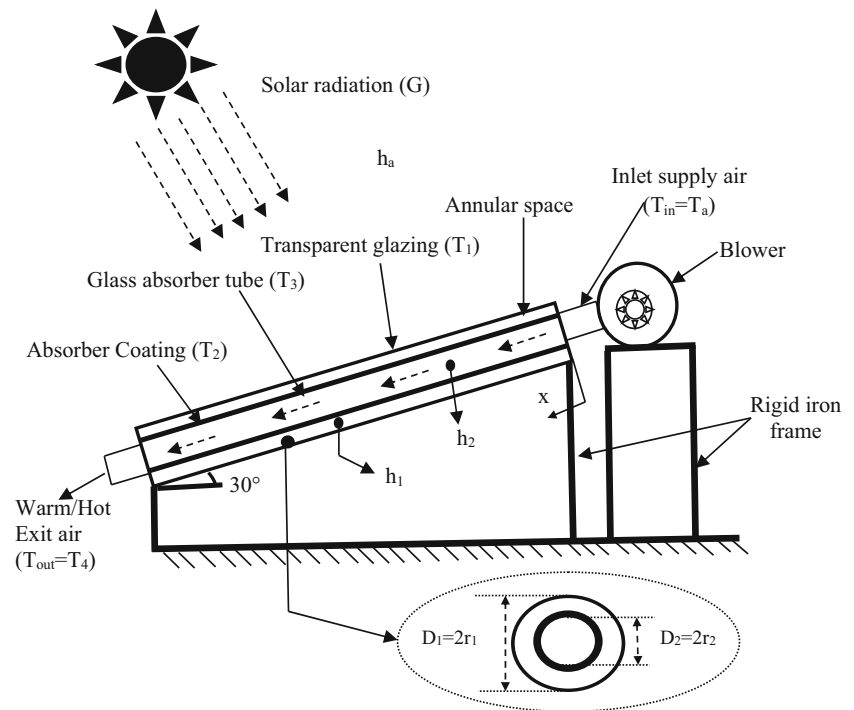
The experimental test was achieved in order to determine the exit air temperature at different parameters. The data were recorded after every half an hour from 8:30 h (morning) to 5:00 h (evening). The results are shown in Fig. 6.

## 5 Validation of the model

In order to verify the accuracy of the model, the comparisons of the simulated results with results given by the experimental test carry out at approximately similar parametric conditions is presented in this section. The parametric values are given in Table 2.

Figure 6 shows the variation of exit air temperature (simulated and experimental data) with time, solar intensity and ambient temperature. It is seen that the modelled values of exit air temperature follow the same trend as the experimentally measured values with good agreement, about 4–5% points. From Fig. 6 it is clearly observed that model slightly overestimate the measured values. A difference between

**Fig. 5** Schematic diagram of experimental setup of concentric coaxial glass tube solar air collector



measured and simulated values is perceived, about 5–6% points, which corresponds to a temperature difference of 1–4 °C. The mismatch between the simulated and experimental results is mainly attributed to experimental errors which are a function of the accuracy of the measurement and unstable weather conditions.

### 6 Results and discussion

The performance of the CCGTSAC was studied over a wide range of thirteen different parameters. Each parameter was varied, keeping the others constant as shown in Table 2. Spatial discretization was performed with thirteen elements located every 0.1 m along the tube. Some of the salient results are discussed below.

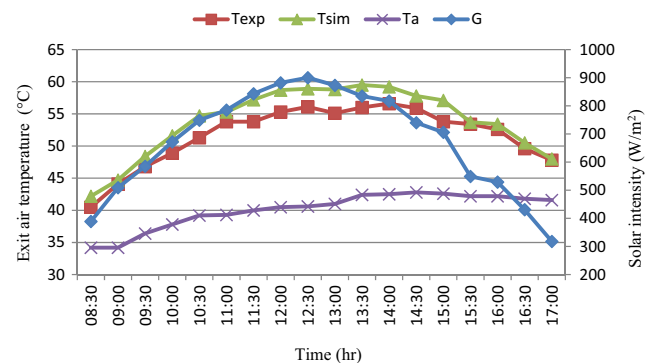
#### 6.1 Effect of transparent glazing size on exit air temperature

Figure 7 indicates that variation of heat absorbed by air with an increase in the intensity of solar radiation. It could be

observed from this figure that at maximum solar intensity, more heat was absorbed by the air. Results found that the exit air temperature difference were measured at  $G = 300 \text{ W/m}^2$ ,  $G = 600 \text{ W/m}^2$  and  $G = 900 \text{ W/m}^2$  were 14.9 °C, 29.8 °C and 44.1 °C when glazing radius was 0.028 m, 14.9 °C, 29.8 °C and 43.9 °C when glazing radius was 0.029 m, 14.9 °C, 29.7 °C and 43.9 °C when glazing radius was 0.030 m, 14.9 °C, 29.6 °C and 43.8 °C when glazing radius was 0.031 m, 14.8 °C, 29.4 °C and 43.7 °C when glazing radius was 0.032 m. That is, transparent glazing size has no significant effect on increasing the exit air temperature. Exit air temperature decreases with an increase in the transparent glazing size because convective heat loss increases between the absorber coating and transparent glazing. So, with increase in the transparent glazing size leads to increase the covered area by the collector with decrease in exit air temperature.

**Table 1** Materials of the CCGT

Name	Material
Transparent glazing	Borosilicate glass
Absorber tube	Borosilicate glass
Absorber coating	Black paint



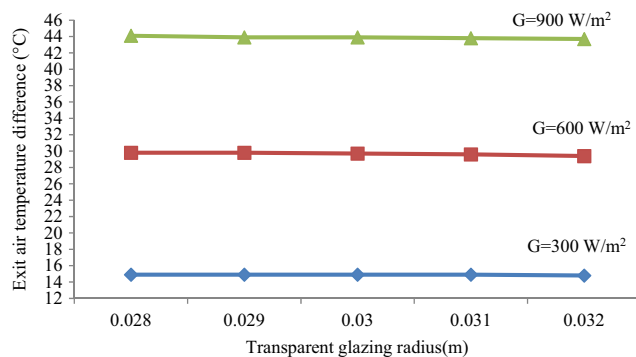
**Fig. 6** Variation of exit air temperature difference with solar intensity: comparison between experimental data and simulation results

**Table 2** Numerical values of the parameters used in the model

Parameters	Fixed values of parameters (during variation of other parameters)	Variation	Units
$r_1$	0.030	0.028–0.032	m
$r_2$	0.019	0.019–0.027	m
$L$	1.2	0.1–1.2	m
$t$	0.002	0.001–0.005	m
$\alpha_1$	0.05	0.05–0.25	–
$\tau_1$	0.9	0.6–0.9	–
$\epsilon_2$	0.91	0.8–0.95	–
$\alpha_2$	0.91	0.75–0.95	–
$T_{in}$ or $T_a$	30	18–42	°C
$\dot{m}$	0.0095	0.008–0.0196	kg/s
$\mu$	$1.87 \times 10^{-5}$	$1.937 \times 10^{-5}$ – $2.029 \times 10^{-5}$	kg/msec
$\rho$	1.158	1.2671–1.0870	kg/m <sup>3</sup>
$\kappa$	0.0266	0.0243–0.0281	W/m°C
$C_p$	1000	1004–1007	J/kg°C
$u_{wind}$	1	1–3	m/s

## 6.2 Effect of absorber tube size on exit air temperature

Figure 8 shows that the size of absorber tube has a strong influence on the thermal performance of CCGT. Results found that the exit air temperatures difference were measured at  $G = 300 \text{ W/m}^2$ ,  $G = 600 \text{ W/m}^2$  and  $G = 900 \text{ W/m}^2$  were 14.9 °C, 29.7 °C and 43.9 °C when absorber tube radius was 0.019 m, 16 °C, 32.2 °C and 47.8 °C when absorber tube radius was 0.021 m, 17.5 °C, 34.5 °C and 51.4 °C when absorber tube radius was 0.023 m, 18.7 °C, 37.1 °C and 55 °C when absorber tube radius was 0.025 m, 20 °C, 39.6 °C and 58.4 °C when absorber tube radius was 0.027 m. As can be seen from the Fig. 6, exit air temperature increases with the increase of the absorber tube size. This is due to the increase of absorber tube size, on one hand, increasing the contact surface between air and absorber tube wall and then resulting in heat transfer enhancement, on the other hand, increasing the external surface

**Fig. 7** Influence of transparent glazing size on exit air temperature difference at different solar intensity

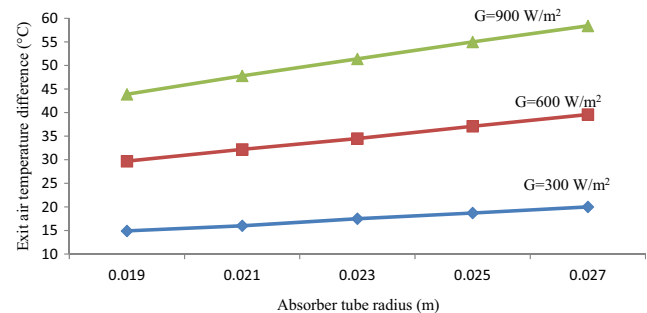
area of the absorber tube so as to increase the effective absorber area and then helping air to absorb more heat.

## 6.3 Effect of length of CCGT on exit air temperature

Figure 9 shows that the length of CCGT has a strong influence on the thermal performance of CCGTSAC. It is found from the Fig. 9 that exit air temperature increases nonlinearly along the axial direction of CCGT. Results found that the exit air temperature difference were measured at  $G = 300 \text{ W/m}^2$ ,  $G = 600 \text{ W/m}^2$  and  $G = 900 \text{ W/m}^2$  were 14.9 °C, 29.7 °C and 43.9 °C for length of CCGT was taken to 1.2 m. This is because absorber surface and resistance time of air increases with an increase in the length of the CCGT.

## 6.4 Effect of thickness of absorber tube on exit air temperature

Figure 10 shows that the air temperature increases with increase of solar irradiation falls on the CCGTSC.

**Fig. 8** Influence of absorber tube size on exit air temperature difference at different solar intensity



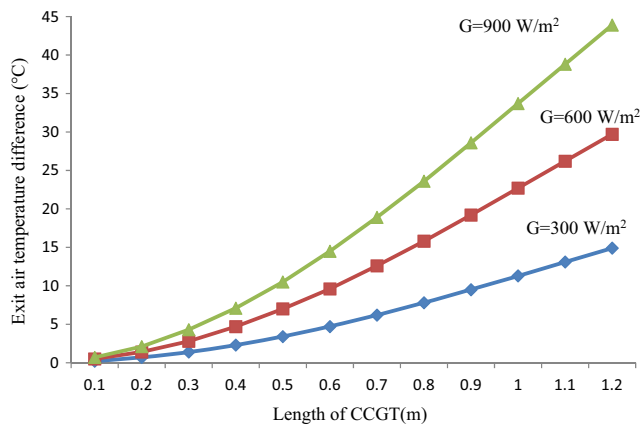


**Fig. 9** Influence of length of CCGT on exit air temperature difference at different solar intensity

Results found that the exit air temperature difference were measured at  $G = 300 \text{ W/m}^2$ ,  $G = 600 \text{ W/m}^2$  and  $G = 900 \text{ W/m}^2$  were  $14.9 \text{ }^\circ\text{C}$ ,  $29.8 \text{ }^\circ\text{C}$  and  $44.1 \text{ }^\circ\text{C}$  when absorber tube thickness was  $0.001 \text{ m}$ ,  $14.9 \text{ }^\circ\text{C}$ ,  $29.7 \text{ }^\circ\text{C}$  and  $43.9 \text{ }^\circ\text{C}$  when absorber tube thickness was  $0.002 \text{ m}$ ,  $14.8 \text{ }^\circ\text{C}$ ,  $29.6 \text{ }^\circ\text{C}$  and  $43.9 \text{ }^\circ\text{C}$  when absorber tube thickness was  $0.003 \text{ m}$ ,  $14.8 \text{ }^\circ\text{C}$ ,  $29.5 \text{ }^\circ\text{C}$  and  $43.7 \text{ }^\circ\text{C}$  when absorber tube thickness was  $0.004 \text{ m}$  and  $14.7 \text{ }^\circ\text{C}$ ,  $29.5 \text{ }^\circ\text{C}$  and  $43.7 \text{ }^\circ\text{C}$  when absorber tube thickness was  $0.005 \text{ m}$  respectively. Results revealed that no significant effect of the thickness of the absorber tube on the performance of CCGTSC because solar radiation falls on the absorber tube was first absorbed by the coating of negligible thickness and then transfer it to the inner surface of the absorber tube by conduction. This heat energy was absorbed by flowing air through convection. The heat transfer coefficient between the absorber tube wall and flowing air was low and solar radiations fall on the absorber tube consistently that's why the temperature of the inner surface of the absorber tube was constant with the variation of the thickness of the absorber tube.

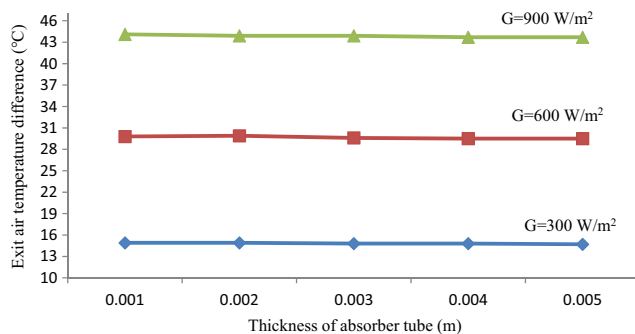


**Fig. 10** Influence of thickness of absorber tube on exit air temperature difference at different solar intensity

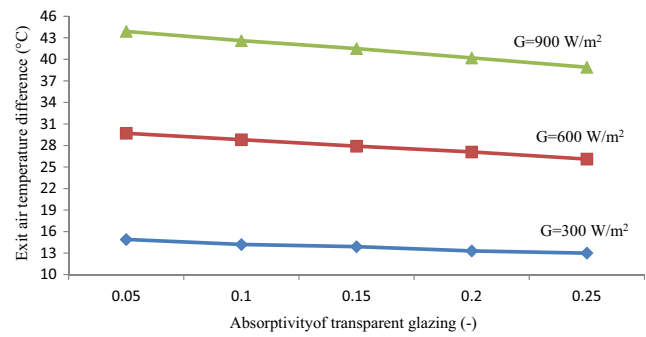


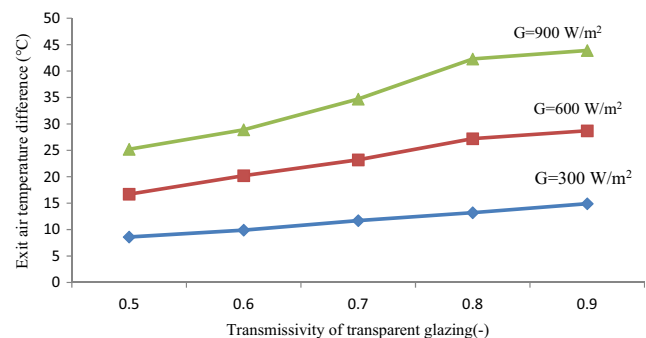
**Fig. 11** Influence of absorptivity of transparent glazing on exit air temperature difference at different solar intensity

### 6.5 Effect of absorptivity of transparent glazing on exit air temperature

Figure 11 shows that temperature difference of exit air were measured at  $G = 300 \text{ W/m}^2$ ,  $G = 600 \text{ W/m}^2$  and  $G = 900 \text{ W/m}^2$  were  $14.9 \text{ }^\circ\text{C}$ ,  $29.7 \text{ }^\circ\text{C}$  and  $43.9 \text{ }^\circ\text{C}$  for  $\alpha_1 = 0.05$ ,  $14.2 \text{ }^\circ\text{C}$ ,  $28.8 \text{ }^\circ\text{C}$  and  $42.6 \text{ }^\circ\text{C}$  for  $\alpha_1 = 0.10$ ,  $13.9 \text{ }^\circ\text{C}$ ,  $27.9 \text{ }^\circ\text{C}$  and  $41.5 \text{ }^\circ\text{C}$  for  $\alpha_1 = 0.15$ ,  $13.3 \text{ }^\circ\text{C}$ ,  $27.1 \text{ }^\circ\text{C}$  and  $40.2 \text{ }^\circ\text{C}$  for  $\alpha_1 = 0.20$  and  $13 \text{ }^\circ\text{C}$ ,  $26.1 \text{ }^\circ\text{C}$  and  $38.9 \text{ }^\circ\text{C}$  for  $\alpha_1 = 0.25$ , respectively. Results revealed that the influence of the absorptivity of transparent glazing on the exit air temperature was significant. Exit air temperature decreases with an increase in the absorptivity of transparent glazing with minimizing the transmissivity by keeping reflectivity constant because the amount of solar intensity reaches to the absorber coating decreases.

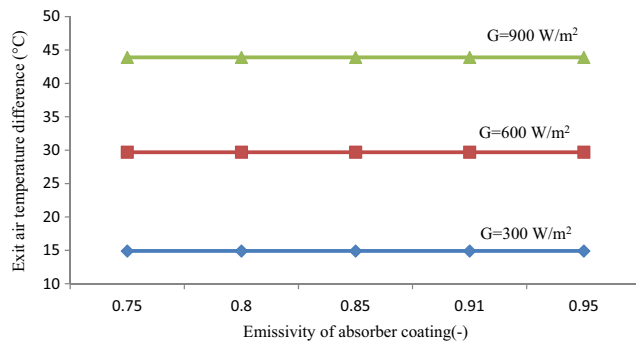
### 6.6 Effect of transmissivity of transparent glazing on exit air temperature

Figure 12 revealed that exit air temperature difference were measured at  $G = 300 \text{ W/m}^2$ ,  $G = 600 \text{ W/m}^2$  and  $G = 900 \text{ W/m}^2$  were  $8.6 \text{ }^\circ\text{C}$ ,  $16.7 \text{ }^\circ\text{C}$  and  $25.2 \text{ }^\circ\text{C}$  at  $\tau_1 = 0.50$ ,  $9.9 \text{ }^\circ\text{C}$ ,  $20.2 \text{ }^\circ\text{C}$  and  $28.2 \text{ }^\circ\text{C}$  at  $\tau_1 = 0.60$ ,  $11.7 \text{ }^\circ\text{C}$ ,  $23.2 \text{ }^\circ\text{C}$  and  $34.7 \text{ }^\circ\text{C}$  at  $\tau_1 = 0.70$  and  $13.2 \text{ }^\circ\text{C}$ ,  $27.2 \text{ }^\circ\text{C}$  and  $42.3 \text{ }^\circ\text{C}$  at



**Fig. 12** Influence of transmissivity of transparent glazing on exit air temperature difference at different solar intensity





**Fig. 13** Influence of emissivity of the absorber coating on exit air temperature difference at different solar intensity

$\tau_1 = 0.80$ , 14.9 °C, 28.7 °C and 43.9 °C at  $\tau_1 = 0.90$ , respectively. The results indicated that the thermal performance of the CCGTSC increases with increase of the transmissivity of the glazing due to increase in useful heat gain. Because with an increase of the transmissivity of the glazing leads to transmit maximum solar radiations through them with minimum reflectivity and maximum solar radiation absorbs by the absorber coating and converted into heat energy.

### 6.7 Effect of emissivity of absorber coating on exit air temperature

Figure 13 revealed that exit air temperature difference on the thermal performance of the CCGTSC were measured at  $G = 300 \text{ W/m}^2$ ,  $G = 600 \text{ W/m}^2$  and  $G = 900 \text{ W/m}^2$  were 14.9 °C, 29.7 °C and 43.9 °C for  $\epsilon_2 = 0.75$ , 14.9 °C, 29.7 °C and 43.9 °C for  $\epsilon_2 = 0.80$ , 14.9 °C, 29.7 °C and 43.9 °C for  $\epsilon_2 = 0.85$ , 14.9 °C, 29.7 °C and 43.9 °C for  $\epsilon_2 = 0.91$  and 14.9 °C, 29.7 °C and 43.9 °C for  $\epsilon_2 = 0.95$ . Results show that the influence of the emissivity of absorber coating was not significant because there was no change in exit air temperature difference with an increase in the emissivity of the absorber coating of the CCGTSC. Due to the presence of the glazing, radiation emitted by the absorber coating in the form of long wavelength which are trapped between the glazing and the absorber coating.

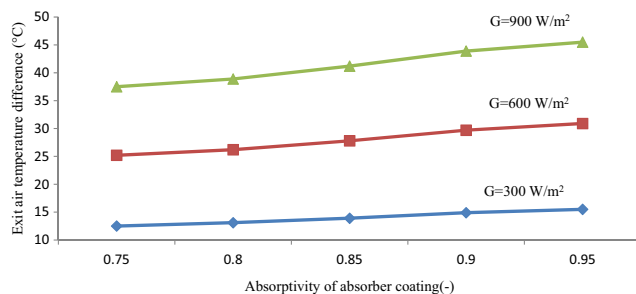


**Fig. 14** Influence of absorptivity of absorber coating on exit air temperature difference at different solar intensity

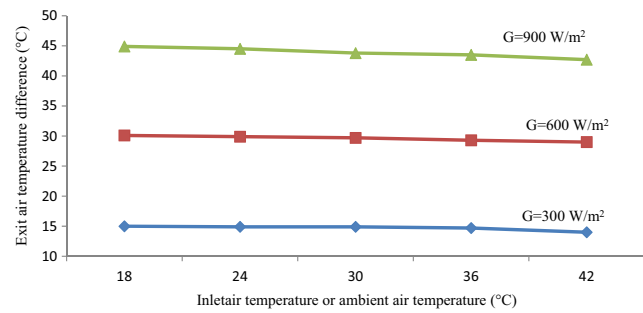


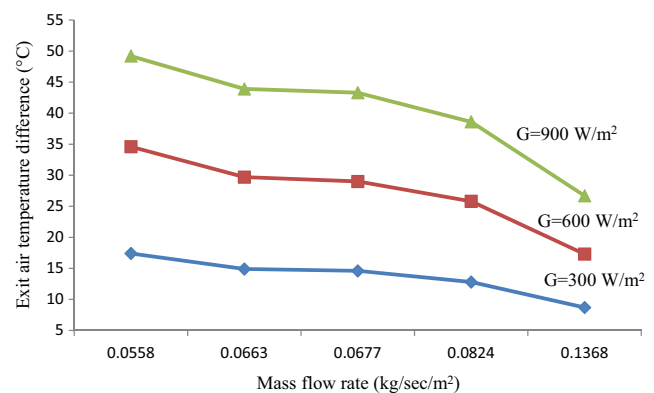
**Fig. 15** Influence of inlet air temperature or ambient air temperature on exit air temperature difference at different solar intensity

### 6.8 Effect of absorptivity of absorber coating on exit air temperature

Figure 14 revealed that exit air temperature difference were measured at  $G = 300 \text{ W/m}^2$ ,  $G = 600 \text{ W/m}^2$  and  $G = 900 \text{ W/m}^2$  were 12.5 °C, 25.2 °C and 37.5 °C at  $\alpha_2 = 0.75$ , 13.1 °C, 26.2 °C and 38.9 °C at  $\alpha_2 = 0.80$ , 13.9 °C, 27.8 °C and 41.2 °C at  $\alpha_2 = 0.85$  and 14.9 °C, 29.7 °C and 43.9 °C at  $\alpha_2 = 0.91$ , 15.5 °C, 30.9 °C and 45.5 °C at  $\alpha_2 = 0.91$ , respectively. The results indicated that the thermal performance of the CCGTSC increases with increase the absorptivity of the absorber coating due to increase in useful heat gain. Because with an increase in the absorptivity of the absorber coating of the CCGT leads to absorb maximum solar radiations and convert into heat energy.

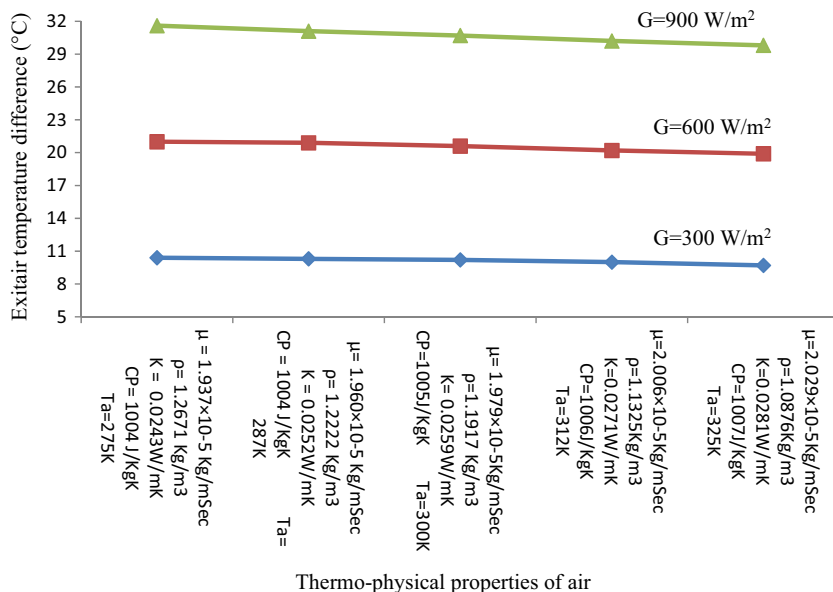
### 6.9 Effect of variation of inlet temperature or ambient temperature of air on exit air temperature

Figure 15 shows that the temperature increases with increase of solar radiation falls on the CCGTSC. In the case where the inlet temperature of the air is the same as the ambient temperature and the results found that the exit air temperature difference were measured at  $G = 300 \text{ W/m}^2$ ,  $G = 600 \text{ W/m}^2$  and  $G = 900 \text{ W/m}^2$  were 15 °C, 30.1 °C and 44.9 °C when  $T_a =$



**Fig. 16** Influence of mass flow rate on exit air temperature difference at different solar intensity

**Fig. 17** Influence of thermo-physical properties of air on exit air temperature difference at different solar intensity



$T_{in}$  was 18 °C, 14.9 °C, 29.9 °C and 44.5 °C when  $T_a = T_{in}$  was 24 °C, 14.9 °C, 29.7 °C and 43.8 °C when  $T_a = T_{in}$  was 30 °C, 14.7 °C, 29.3 °C and 43.5 °C when  $T_a = T_{in}$  was 36 °C, 14 °C, 29 °C and 42.7 °C when  $T_a = T_{in}$  was 42 °C. The results revealed that the exit air temperature difference decreases with increase in inlet air temperature or ambient air temperature, especially, for the larger values. Because when inlet air temperature increase leads to decrease the temperature gradient between the absorber tube wall and air flowing through the absorber tube. So, less amount of heat exchange takes place.

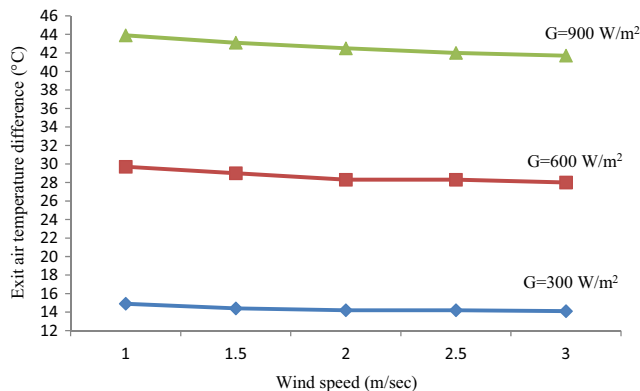
**6.10 Effect of mass flow rate on exit air temperature**

Figure 16 shows that the exit air temperature difference were measured at  $G = 300 \text{ W/m}^2$ ,  $G = 600 \text{ W/m}^2$  and  $G = 900 \text{ W/m}^2$  were 17.4 °C, 34.6 °C and 49.2 °C for  $\dot{m} = 0.0558 \text{ kg/s/m}^2$ , 14.9 °C, 29.7 °C and 43.9 °C for  $\dot{m} = 0.0663 \text{ kg/s/m}^2$ , 14.6 °C, 29 °C and 43.3 °C for  $\dot{m} = 0.0677 \text{ kg/s/m}^2$ , 12.3 °C, 25.8 °C and 38.6 °C for  $\dot{m} = 0.0824 \text{ kg/s/m}^2$  and 8.7 °C, 17.3 °C and 26.7 °C for  $\dot{m} = 0.1368 \text{ kg/s/m}^2$ . Results revealed that a remarkable fall in the exit air temperature with increase in mass flow rate. This is due to increase in the heat capacity of air at same solar heat input and leads to less resistant time of the air to take heat from heated absorber tube wall. Hence, the exchange of heat between the air and absorber tube wall decreases with increase in mass flow rate of air. So, high flow rates are not recommended for the better performance of the CCGTSC.

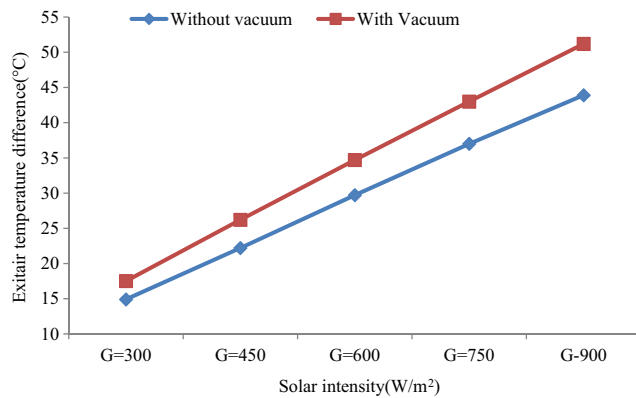
**6.11 Effect of variation of thermo-physical properties of air on exit air temperature**

Figure 17 shows that exit air temperatures were measured at  $G = 300 \text{ W/m}^2$ ,  $G = 600 \text{ W/m}^2$  and  $G = 900 \text{ W/m}^2$  were

10.4 °C, 21 °C and 31.6 °C when considering thermo-physical properties of air at  $T_a = 18 \text{ °C}$  and 10.3 °C, 20.9 °C and 31.1 °C when considering thermo-physical properties of air at  $T_a = 24 \text{ °C}$ , 10.2 °C, 20.6 °C and 30.7 °C when considering thermo-physical properties of air at  $T_a = 30 \text{ °C}$ , 10 °C, 20.2 °C and 30.2 °C when considering thermo-physical properties of air at  $T_a = 36 \text{ °C}$ , 9.7 °C, 19.9 °C and 29.8 °C when considering thermo-physical properties of air at  $T_a = 42 \text{ °C}$ . Results revealed that the density of the air increases with an increase in the temperature of the air, but viscosity, thermal conductivity and specific heat of air decreases with an increase in the temperature of air. Due to this variation in the thermo-physical properties of the air lead to decrease in the exit air temperature difference as compared to exit air temperature difference obtained with constant thermo-physical properties at different inlet air temperature. Hence, thermo-physical properties play an important role to enhance the thermal performance of the CCGTSC.



**Fig. 18** Influence of wind speed on exit air temperature difference at different solar intensity



**Fig. 19** Influence of vacuum present between absorber glass tube and transparent glazing on exit air temperature difference at different solar intensity

### 6.12 Effect of wind speed on exit air temperature

Figure 18 revealed that exit air temperature difference were measured at  $G = 300 \text{ W/m}^2$ ,  $G = 600 \text{ W/m}^2$  and  $G = 900 \text{ W/m}^2$  were  $14.9 \text{ }^\circ\text{C}$ ,  $29.7 \text{ }^\circ\text{C}$  and  $43.9 \text{ }^\circ\text{C}$  at  $u_{\text{wind}} = 1 \text{ m/Sec}$ ,  $14.4 \text{ }^\circ\text{C}$ ,  $29 \text{ }^\circ\text{C}$  and  $43.1 \text{ }^\circ\text{C}$  at  $u_{\text{wind}} = 1.5 \text{ m/Sec}$  and  $14.2 \text{ }^\circ\text{C}$ ,  $28.3 \text{ }^\circ\text{C}$  and  $42.5 \text{ }^\circ\text{C}$  at  $u_{\text{wind}} = 2 \text{ m/Sec}$  and  $14.2 \text{ }^\circ\text{C}$ ,  $28 \text{ }^\circ\text{C}$  and  $42 \text{ }^\circ\text{C}$  at  $u_{\text{wind}} = 2.5 \text{ m/Sec}$  and  $14.1 \text{ }^\circ\text{C}$ ,  $28 \text{ }^\circ\text{C}$  and

$41.7 \text{ }^\circ\text{C}$  at  $u_{\text{wind}} = 3 \text{ m/Sec}$  respectively. The results indicated that wind speed has no significant influence on the thermal performance of the CCGTSC because to reduce the effect of wind speed on the CCGTSC provides transparent glazing on the absorber tube for minimizing the convective heat losses due to direct contact with the wind.

### 6.13 Effect of vacuum present between the absorber glass tube and transparent glazing on exit air temperature

Figure 19 shows vacuum present between the absorber glass tube and transparent glazing has a significant effect on the thermal performance of CCGTSAC. Figure revealed that exit air temperature difference were measured at  $G = 300 \text{ W/m}^2$ ,  $G = 450 \text{ W/m}^2$ ,  $G = 600 \text{ W/m}^2$ ,  $G = 750 \text{ W/m}^2$  and  $G = 900 \text{ W/m}^2$  were  $14.9 \text{ }^\circ\text{C}$ ,  $22.2 \text{ }^\circ\text{C}$ ,  $29.7 \text{ }^\circ\text{C}$ ,  $37 \text{ }^\circ\text{C}$  and  $43.9 \text{ }^\circ\text{C}$  when collector operates at without vacuum condition but  $17.5 \text{ }^\circ\text{C}$ ,  $26.2 \text{ }^\circ\text{C}$ ,  $37.5 \text{ }^\circ\text{C}$ ,  $43 \text{ }^\circ\text{C}$  and  $51.2 \text{ }^\circ\text{C}$  when collector operates at with vacuum conditions. Results show that the vacuum condition gives better results as compared to without vacuum condition because convective losses between the absorber coating to transparent glazing decreases with the

**Table 3** Comparison of simulation results of present study with past studies

S.No.	Parameter study	Present study	Past studies
1	Effect of solar radiation	Exit air temperature increases with increase in solar intensity	Heat gain by working fluid increases with increase in solar intensity [30]
2	Effect of transparent glazing size	Glazing size do not significantly influence the gain of temperature by exit air	
3	Effect of absorber tube size	Absorber tube size has a strong influence to raise the exit air temperature	
4	Effect of length of tube	Length of tube has a strong influence to raise the exit air temperature	
5	Effect of absorptivity of transparent glazing	Absorptivity of glazing has a strong influence on heat gain by exit air temperature	
6	Effect of transmissivity of transparent glazing	Transmissivity of glazing has a strong influence on heat gain by exit air temperature	
7	Effect of absorptivity of absorber coating	Absorptivity of absorber coating has a strong influence on heat gain by exit air temperature	
8	Effect of emissivity of absorber coating	Emissivity of absorber coating do not effect on heat gain by exit air temperature because absorber coating temperature is not so high	At higher exit air temperature, emissivity has a significant impact on the thermal performance of the collector [2, 20]
9	Effect of ambient temperature/ inlet temperature	Ambient temperature/ inlet air temperature has a strong of exit influence to raise the temperature air	Heat gain by the fluid decreases with increase in the inlet temperature of the fluid [30, 40]
10	Effect of mass flow rate	Exit air temperature decreases with increase in mass flow rate of air	Heat gain by working fluid decreases with increase in mass flow rate of fluid [36–38]
11	Effect of thermo-physical properties of air	Thermo-physical properties of air has a strong influence on heat gain by exit air temperature	
12	Effect of wind speed	Wind speed do not influence the gain of temperature by exit air	
13	Effect of vacuum	Vacuum has a strong effect on the temperature gain by exit air	Performance of the collector increases with present of vacuum [19, 39]

presence of vacuum. This leads to increase the surface temperature of the absorber coating and transfer more heat to the air as compared to without vacuum condition.

Table 3 presents a comparison of model results of the present study with the simulation results in the literature. Through many results of earlier studies that have the same objectives are comparable, there are additional results from the simulation presented here, especially those related to the influence of performance solar radiation, mass flow rate, wind speed, thermo-physical properties of air, ambient temperature/ inlet temperature. Some other outputs could not be compared as similar information is not available in the literature.

## 7 Conclusions

A mathematical model based on energy balance equations for CCGT has been developed to predict its thermal behaviour over a wide range of different parameters. Results of the model were used to show the effects of key parameters on the performance of a CCGTSAC for an exit air temperature difference of 14.9 °C to 58.4 °C, aimed at its use as solar air heater for various domestic and industrial applications. In conclusion, the main results from this paper are summarized below:

- Exit air temperature increases with increase in solar intensity and become maximum when the solar intensity is maximum.
- The absorber tube size has the strong effect on the exit air temperature instead of transparent glazing size.
- Exit air temperature increases with increase in the length of CCGT.
- When the thickness of the absorber tube is increased, the strength of the tube increases without significant influence the exit air temperature.
- Ambient temperature or inlet air temperature has the strong effect on the exit air temperature instead of wind speed.
- Exit air temperature decreases with increase in the air mass flow rate. Low mass flow rate is used to obtain high exit air temperature.
- Absorptivity of transparent glazing and absorber coating has strong effect on the exit air temperature. Exit air temperature decreases with increase in absorptivity of the transparent glazing but increases with increase in absorptivity of the absorber coating.
- The emissivity of absorber coating has no significant effect on the exit air temperature but increases with increase in transmissivity of the glazing have strong effect on the exit air temperature.

- CCGTSAC gives better results in case of vacuum present between absorber tube and transparent glazing as compare to no vacuum condition.

## 7.1 Future scope

For domestic and industrial applications, a modified system can be developed to minimize the overall cost and to improve the efficiency of the CCGTSAC by using all significant parameters.

## References

1. Lamnatou C, Papanicolaou E, Belessiotis V, Kyriakis N (2012) Experimental investigation and thermodynamic performance analysis of a solar dryer using an evacuated-tube air collector. *Appl Energy* 94:232–243. <https://doi.org/10.1016/j.apenergy.2012.01.025>
2. Wang PY, Guan HY, Liu ZH, Wang GS, Zhao F, Xiao HS (2014) High temperature collecting performance of a new all-glass evacuated tubular solar air heater with U-shaped tube heat exchanger. *Energy Convers Manag* 77:315–323. <https://doi.org/10.1016/j.enconman.2013.08.019>
3. Njomo D (2000) Unglazed selective absorber solar air collector: heat exchange analysis. *Heat Mass Transf* 36(4):313–317. <https://doi.org/10.1007/s002310000084>
4. Tchinda R (2008) Thermal behaviour of solar air heater with compound parabolic concentrator. *Energy Convers Manag* 49:529–540. <https://doi.org/10.1016/j.enconman.2007.08.004>
5. Akhtar N, Mullick SC (1999) Approximate method for computation of glass cover temperatures and top heat loss coefficient of solar collectors with single glazing. *Sol Energy* 66:349–354. [https://doi.org/10.1016/S0038-092X\(99\)00032-8](https://doi.org/10.1016/S0038-092X(99)00032-8)
6. Chemkhi S, Zagrouba F, Bellagi A (2004) Drying of agricultural crops by solar energy. *Desalination* 168:101–109. <https://doi.org/10.1016/j.desal.2004.06.174>
7. Akpınar EK, Kocyyigit F (2010) Experimental investigation of thermal performance of solar air heater having different obstacles on absorber plates. *Int Commun Heat Mass Transfer* 37:416–421. <https://doi.org/10.1016/j.icheatmasstransfer.2009.11.007>
8. Sahin AS (2012) Optimization of solar air collector using genetic algorithm and artificial bee colony algorithm. *Heat Mass Transf* 48(11):1921–1928. <https://doi.org/10.1007/s00231-012-1038-2>
9. Yang M, Wang P, Yang X, Shan M (2012) Experimental analysis on thermal performance of a solar air collector with a single pass. *Build Environ* 56:361–369. <https://doi.org/10.1016/j.buildenv.2012.04.009>
10. Kumar K, Prajapati DR, Samir S (2017) Heat transfer and friction factor correlations development for solar air heater duct artificially roughened with ‘S’ shape ribs. *Exp Thermal Fluid Sci* 82:249–261. <https://doi.org/10.1016/j.expthermflusci.2016.11.012>
11. Gill RS, Hans VS, Saini JS, Singh S (2017) Investigation on performance enhancement due to staggered piece in a broken arc rib roughened solar air heater duct. *Renew Energy* 104:148–162. <https://doi.org/10.1016/j.renene.2016.12.002>
12. Harding GL, Window B (1981) Thermal conduction in evacuated concentric tubular solar energy collectors degraded by low pressure

- gas. *Sol Energy Mater* 4:421–434. [https://doi.org/10.1016/0165-1633\(81\)90018-6](https://doi.org/10.1016/0165-1633(81)90018-6)
13. El-Nashar AM (2009) Seasonal effect of dust deposition on a field of evacuated tube collectors on the performance of a solar desalination plant. *Desalination* 239:66–81. <https://doi.org/10.1016/j.desal.2008.03.007>
  14. Tang R, Yang Y, Gao W (2011) Comparative studies on thermal performance of water-in-glass evacuated tube solar water heaters with different collector tilt-angles. *Sol Energy* 85:1381–1389. <https://doi.org/10.1016/j.solener.2011.03.019>
  15. Gao Y, Fan R, Zhang XY, YJ AN, Wang MX, Gao YK, Yu Y (2014) Thermal performance and parameter analysis of a U-pipe evacuated solar tube collector. *Sol Energy* 107:714–727. <https://doi.org/10.1016/j.solener.2014.05.023>
  16. Kim Y, Seo T (2007) Thermal performances comparisons of the glass evacuated tube solar collectors with shapes of absorber tube. *Renew Energy* 32:772–795. <https://doi.org/10.1016/j.renene.2006.03.016>
  17. Ma L, Lu Z, Zhang J, Liang R (2010) Thermal performance analysis of the glass evacuated tube solar collector with U-tube. *Build Environ* 45:1959–1967. <https://doi.org/10.1016/j.buildenv.2010.01.015>
  18. Fischer S, Frey P, Druck H (2012) A comparison between state-of-the-art and neural network modelling of solar collectors. *Sol Energy* 86:3268–3277. <https://doi.org/10.1016/j.solener.2012.09.002>
  19. Ares-Muzio O, Lizama-Tzec I, Macias JD, Oskam G, Cahue A, De Coss R, Alvarado-Gil JJ, Cortes C (2014) Characterization of thermal losses in an evacuated tubular solar collector prototype for medium temperature applications. *Energy Procedia* 57:2121–2130. <https://doi.org/10.1016/j.egypro.2014.10.177>
  20. Wang PY, Li SF, Liu ZH (2015) Collecting performance of an evacuated tubular solar high-temperature air heater with concentric tube heat exchanger. *Energy Convers Manag* 106:1166–1173. <https://doi.org/10.1016/j.enconman.2015.10.058>
  21. Hall R, Blower J (2016) Low-emissivity transpired solar collectors. *Energy Procedia* 91:56–63. <https://doi.org/10.1016/j.egypro.2016.06.171>
  22. Dabra V, Yadav L, Yadav A (2013) The effect of tilt angle on the performance of evacuated tube solar air collector: experimental analysis. *Int J Eng Sci Technol* 5:100–110. <https://doi.org/10.4314/ijest.v5i4.9>
  23. Garcia-Valladares O, Velazquez N (2009) Numerical simulation of parabolic trough solar collector: improvement using counter flow concentric circular heat exchangers. *Int J Heat Mass Transf* 52:597–609. <https://doi.org/10.1016/j.ijheatmasstransfer.2008.08.004>
  24. Li M, Wang LL (2006) Investigation of evacuated tube heated by solar trough concentrating system. *Energy Convers Manag* 47:3591–3601. <https://doi.org/10.1016/j.enconman.2006.03.003>
  25. Zhang XR, Yamaguchi H (2008) An experimental study on evacuated tube solar collector using supercritical CO<sub>2</sub>. *Appl Therm Eng* 28:1225–1233. <https://doi.org/10.1016/j.applthermaleng.2007.07.013>
  26. Zhao C, You S, Wei L, Gao H, Yu W (2016) Theoretical and experimental study of the heat transfer inside a horizontal evacuated tube. *Sol Energy* 132:363–372. <https://doi.org/10.1016/j.solener.2016.03.016>
  27. Shah LJ, Furbo S (2007) Theoretical flow investigations of an all glass evacuated tubular collector. *Sol Energy* 81:822–828. <https://doi.org/10.1016/j.solener.2006.09.007>
  28. Gulcimen F, Karakaya H, Durmus A (2016) Drying of sweet basil with solar air collectors. *Renew Energy* 93:77–86. <https://doi.org/10.1016/j.renene.2016.02.033>
  29. Yadav A, Bajpai VK (2012) Thermal performance of one-ended evacuated tube solar air collector at different flow rates: experimental investigation. *Int J Ambient Energy* 33:35–50. <https://doi.org/10.1080/01430750.2011.636207>
  30. Naik BK, Varshney A, Muthukumar P, Somayaji C (2016) Modelling and performance analysis of U type evacuated tube solar collector using different working fluids. *Energy Procedia* 90:227–237. <https://doi.org/10.1016/j.egypro.2016.11.189>
  31. Sukhatme SP (2005) *Solar energy principles of thermal collection and storage*, 2nd edn. TMH, New Delhi
  32. Estrada-Gasca CA, Garcia GA, Cabanillas RE, Nair PK (1992) Theoretical analysis of the thermal performance of all-glass evacuated tube solar collectors with absorber coating on the outside or inside of the inner tube. *Renew Energy* 2:477–483. [https://doi.org/10.1016/0960-1481\(92\)90084-G](https://doi.org/10.1016/0960-1481(92)90084-G)
  33. Tong Y, Kim J, Cho H (2015) Effects of thermal performance of enclosed-type evacuated U-tube solar collector with multi-walled carbon nanotube/water nanofluid. *Renew Energy* 83:463–473. <https://doi.org/10.1016/j.renene.2015.04.042>
  34. Gnielinski V (1976) New equations for heat and mass transfer in turbulent pipe and channel flow. *Int Chem Eng* 16:359–368
  35. Ong KS (1995) Thermal performance of solar air heaters: mathematical model and solution procedure. *Sol Energy* 55:93–109. [https://doi.org/10.1016/0038-092X\(95\)00021-I](https://doi.org/10.1016/0038-092X(95)00021-I)
  36. Zhu TT, Diao YH, Zhao YH, Deng YC (2015) Experimental study on the thermal performance and pressure drop of a solar air collector based on flat micro-heat pipe arrays. *Energy Convers Manag* 94:447–457. <https://doi.org/10.1016/j.enconman.2015.01.052>
  37. Ersoz MA (2016) Effects of different working fluid use on the energy and exergy performance for evacuated tube solar collector with thermosyphon heat pipe. *Renew Energy* 96:244–256. <https://doi.org/10.1016/j.renene.2016.04.058>
  38. Daghigh R, Shafieian A (2016) Energy-exergy analysis of a multi-purpose evacuated tube heat pipe solar water heating-drying system. *Exp Thermal Fluid Sci* 78:266–277. <https://doi.org/10.1016/j.expthermflusci.2016.06.010>
  39. Sharma N, Diaz GG (2011) Performance model of a novel evacuated-tube solar collector based on minichannels. *Sol Energy* 85:881–890. <https://doi.org/10.1016/j.solener.2011.02.001>
  40. Daghigh R, Shafieian A (2016) An experimental study of a heat pipe evacuated tube solar dryer with heat recovery system. *Renew Energy* 96:872–880. <https://doi.org/10.1016/j.renene.2016.05.025>